Dalton Transactions

Spectroscopic and Crystallographic Anomalies of (Co1-xZnx)Al2O4 Spinel Oxide

Journal:	*Dalton Transactions*
Manuscript ID:	DT-ART-05-2014-001599.R1
Article Type:	Paper
Date Submitted by the Author:	29-Sep-2014

Complete List of Authors:	Nakane, Takayuki; National Institute for Materials Science, Naka, Takashi; National Institute for Materials Science, Sato, Koichi; Tohoku University, Institute of Multidisciplinary Research for Advanced Materials Taguchi, Minori; Chuo University, Applied Chemistry Nakayama, Minako; National Institute for Materials Science, Mitsui, Tadashi; National Institute for Materials Science, Matsushita, Akiyuki; National Institute for Materials Science, Chikyow, Toyohiro; National Institute for Materials Science (NIMS),

Journal Name

RSCPublishing

ARTICLE

Spectroscopic and Crystallographic Anomalies of $(Co_{1-x}Zn_x)Al_2O_4$ Spinel Oxide

Cite this: DOI: 10.1039/xoxxoooooox

Takayuki Nakane,[a] Takashi Naka[1], Koichi Sato,[b] Minori Taguchi,[c] Minako Nakayama,[a] Tadashi Mitsui,[a] Akiyuki Matsushita[a] and Toyohiro Chikyow[a] ,

Received ooth January 2012,
Accepted ooth January 2012

DOI: 10.1039/xoxxoooooox

www.rsc.org/

A This work investigates the spectroscopic properties of $(Co_{1-x}Zn_x)Al_2O_4$ with the wide range x of $0 \le x \le 1$. Spectroscopic and crystallographic evaluations using XRD, Raman, FT-IR and UV-VIS spectroscopy reveals that the Zn^{2+} substitution systematically changes the lattice constant depending on the Co-O bond mainly and the related optical characteristics of this material. The x dependence of these properties has two trends, and the mutational point seems to exist at around $x \approx 0.5$. Implying that the electronic structure of $(Co_{1-x}Zn_x)Al_2O_4$ is not changed monotonically by this Zn^{2+} substitution. Interestingly, some optical phenomena found in this study become prominent for the sample of $x \ge 0.5$. That is, we found the sideband peaks near the main peak of the Raman spectra, and the relative intensities of them systematically and sensitively increased with Zn^{2+} substitution proceeds. The increasing rates are not constant, and it becomes to be high for the sample of $x \ge 0.5$. These sideband peaks are considered reflecting the unique change in the local electronic structure of $(Co_{1-x}Zn_x)Al_2O_4$, and they are useful for evaluating the substitution level without the influence of the site change phenomenon. Thus, clarifying them is expected to be important issue for understanding and controlling the electronic structure of the spinel oxide. On the other hand, discussion for the visible light absorption of the *d-d* transition of Co^{2+} reveals that the efficiency also becomes to be high for the sample with high Zn^{2+} substitution ($x \ge 0.5$). This is also considered as the valuable information for the investigation of the optical property and/or the catalytic function of the spinel oxide. Moreover, the spectroscopic characteristics considered as the fluorescence of $(Co_{1-x}Zn_x)Al_2O_4$ samples is also identified as the novel functional property of this material. The intensity of this fluorescence peak also drastically becomes to be high for the sample of $x \ge 0.7$. The effect of Zn^{2+} substitution on the local electronic structure of $(Co_{1-x}Zn_x)Al_2O_4$ has not been cleared, yet. However, some interesting characteristics reviewed in this study are worth investigating from the viewpoint of the material science and its application.

Introduction

Spinel is one of the famous structures, and the oxide materials are widely investigated in some scientific fields like solid-state physics and catalytic chemistry, optical science, inorganic material fields. [1–3] The normal spinel oxide is described as AB_2O_4 compositional formula, where A and B are the sites occupied by di- and trivalent metal cations, respectively. The importance of the spinel oxide is that these two different sites form tetrahedral (T_d: A site) and octahedral (O_h: B site) structures with the O^{2-} as the coordination anion. This structural characteristic provides numerous attractive properties of a lot of spinel oxides. Among spinel materials, cobalt aluminate ($CoAl_2O_4$) is well known as Thenard's blue pigment widely used in the ceramic industry as coloring agents in glazes and porcelain stoneware because of its thermal and chemical stability.[4–6] In this case, Co^{2+} at the A site is of significance, and the blue color originates in the *d-d* transition of this cation in the T_d structure. That is, d orbits of Co^{2+} at A site in $CoAl_2O_4$ spinel oxide splits into a low-lying doublets (E_g orbital) and a higher triplets (T_{2g} orbital) by the crystal field with T_d symmetry (ligand field splitting),[7] and this energy gap corresponding to about 1.8 eV (688 nm) absorbs the visible light (*d-d* transition).[8-11] In the meanwhile, $CoAl_2O_4$ is recently focused as the heterogeneous catalyst for the methane reformation and/or as the catalyst for photoelectochemical splitting of H_2O.[12–15] This case also value the energy gap of the *d-d* transition for its photo absorption ability. Furthermore, the Co^{2+} at A site has a high spin state ($S = 3/2$) with an electronic configuration ($E_g^4T_{2g}^3$), and thus the magnetic property of $CoAl_2O_4$ is also paid to attention from the viewpoint of the system with frustrated exchange interactions.[16–20] All these discussions fundamentally emphasize the influence of Co^{2+} at the A site on the physical characteristics of $CoAl_2O_4$. Therefore, the investigation for the $CoAl_2O_4$ frequently discusses the cation-exchange-phenomenon between Co^{2+} at the T_d site and Al^{3+} at the O_h site.[21] The degree of this site exchange is defined as the inversion parameter, α, meaning the distribution-degree of Co^{2+} in the B site, i.e. α of $(Co^{2+}_{1-\alpha}Al^{3+}_{\alpha})(Al^{3+}_{2-\alpha}Co^{2+}_{\alpha})O_4$ composition.[22,23] Preparation of $CoAl_2O_4$ often pays attention to decrease this α value. Recently, we

succeeded in a rapid and simple fabrication of $CoAl_2O_4$ by using a hydroxide precursor synthesized by coprecipitation of cobalt and aluminum nitrates in an alkaline solution.[24-26] This precursor enabled low temperature fabrication, but the inversion parameter of the samples sintered at the temperature below 1000 °C was all much higher than 0.1. Fabrication of $CoAl_2O_4$ still requires the efforts to decrease the α value and the disorders in the products.

For the preparation of $CoAl_2O_4$, partial substitution of Zn^{2+} to Co^{2+} site is known as one of the effective way to decrease the inversion parameter.[27-29] Thus, this Zn^{2+} substitution can be expected to control the site exchange phenomena between the T_d and the O_h sites for optimizing the physical characteristics of $CoAl_2O_4$. For instance, $CoAl_2O_4$ with low α value less than 0.1 is expected to become clear blue pigment and to show excellent catalytic property. Moreover, the Zn^{2+} substitution contributes to reduce the spin liquid state arising from geometrical frustration in antiferromagnetic interactions between Co^{2+} cations.[20,30,31] Therefore, $(Co_{1-x}Zn_x)Al_2O_4$ system are thought to be attractive material for the application of the physical properties of $CoAl_2O_4$. However, there are few reports showing the relationship between the Zn^{2+} substitution level and the physical properties of $(Co_{1-x}Zn_x)Al_2O_4$ systematically for the wide range x of $0 \le x \le 1$.

Additionally, application form of these materials will not be only the polycrystalline bulk and/or the powder, but also the other sample form, like nanoparticles,[25,26,32-34] thin film[35] and single crystal. Then, the fabrication techniques of them are generally difficult to control the cation composition, even though it is the key point for the application of $(Co_{1-x}Zn_x)Al_2O_4$ and the related materials. At least, there is not the effective method to evaluate the substitution level of the Zn^{2+} with distinguishing the influence of the site exchange phenomena. Thus, if there are systematic experimental data providing the information about the Zn^{2+} substitution level and the physical properties of $(Co_{1-x}Zn_x)Al_2O_4$ for the wide range x of $0 \le x \le 1$, they should become to be valuable reference for the investigation about the fabrication technique to optimize the physical characteristics of this material. Especially, these reference data are required for the spectroscopic measurements, because they are often non-destructive experiments and useful for some sample forms mentioned above.

Therefore, this study fabricate $(Co_{1-x}Zn_x)Al_2O_4$ series with wide range x ($0 \le x \le 1$) and evaluated them by using the XRD, UV-VIS, FT-IR and Raman spectroscopy in order to provide the reference data for verifying the effects of Zn^{2+} substitution on the spectroscopic properties of this spinel oxide. This is considered as the first systematic approach performing these some predominant and non-destructive measurements for the same sample of $(Co_{1-x}Zn_x)Al_2O_4$ series with wide range x. Then, this study found some interesting phenomena thought to be novel functional properties of this sample series. They are believed to inspire the future investigation for the $(Co_{1-x}Zn_x)Al_2O_4$ and the related materials. Thus, we report and review these obtained systematic results.

Experimental

The samples of $(Co_{1-x}Zn_x)Al_2O_4$ were fabricated from the starting materials of CoO (Kojunndo Chemical Laboratory: 99.9%), ZnO (Nanotech: 1μm) and Al_2O_3 (Furuuchi Chemical: 99.99). They were mixed with the nominal ratio of controlled x ($0 \le x \le 1$) in an agate mortar and pressed into pellet form with the size of about 10 ϕ × 5 mm. The pelletized mixture was placed in the capped alumina crucible (99.9%) and sintered in a furnace under normal air. The temperature was heated up to 1300 °C for 3 hours, kept for 24 hours and cooled down to room temperature slowly for 36 hours. These samples were crushed into powder form except for the Raman spectroscopy measurement.

The lattice constant and some structural information are analyzed from the powder X-Ray Diffraction (XRD) patterns recorded by RINT-2500 diffractometer (Rigaku) using Cu Kα radiation (the wavelength λ_x = 1.542 Å). XRD patterns were plotted against 2θ or d appropriately, where 2θ and d were diffraction angle and lattice spacing, respectively. They are correlated as the equation $\lambda_x = 2d\sin\theta$. Moreover, this study sometimes used the XRD data refined by Rietveld analysis.[36] The XRD data for the Rietveld analysis were measured at the Synchrotron XRD of the Spring-8 at Harima in Japan. Details of refinement process will be described in elsewhere.[37] This study only uses the results, and thus limit the discussion to be about the general trend from x = 0 to x = 1.0. The refined data are also used for the bond valence sum (BVS) calculation[38] in order to discuss the valence state of the cations and the anion. In the BVS method, the bond-valence, s_{ij}, of the bond between species i and j in a solid matrix is calculated from the experimental bond length, r_{ij}, according to the equation $s_{ij} = \exp[(r_0 - r_{ij})/B]$, where B is an empirically determined parameter and has been suggested to be 0.37 Å. Then, the BVS around species i is described as $V_i = \pm\Sigma_j s_{ij}$ in which a positive/negative value is given to a cation/anion, respectively.

The structural change by Zn^{2+} substitution of $(Co_{1-x}Zn_x)Al_2O_4$ is also identified from the micro-Raman Spectroscopy (RS) measured by NanoFinder-1000 (Tokyo Instrument). The incident light was the semiconductor laser with the wave length of 532 nm focused on the sample surface with the diameter smaller than 3μm and intensity smaller than 10 mW/cm^2. The measurement was performed for 20 seconds, and the data was corrected as the integrated counts of three times measurements. For the RS, this study evaluates the energy of light, E, of detected scattered light using equations as follows. The Raman shift, R, was defined as $R = 1/\lambda_i - 1/\lambda_s$, where λ_i is wave length of incident light (= 532×10^{-7} cm) and λ_s is that of detected scattered light. The E is calculated as the $E = hc/e\lambda$, where h, c, e and λ are planck's constant, velocity of light, electrical charge and wave length, respectively.

Local structure of the sample was speculated from the results of Transmission Electron Microscopy (TEM) observation using TEM-2000F (Japan Electron) with the accelerating voltage of 200 kV. On the other hand, absorptions and emission of light were evaluated from powder diffuse reflectance spectra of Fourier transform infrared (FT-IR) spectra recorded by FT/IR-6200 (JASCO) with KBr pellets, Ultraviolet-Visible Spectroscopy (UV-VIS) recorded by V-650 spectrophotometer (JASCO) and of Photoluminescence (PL) spectroscopy recorded by FP-6500 fluorescence spectrometer (JASCO). The obtained spectra of FT-IR and UV-VIS measurements were converted to the absorption spectra using the Kubelka−Munk calculation.[39]

The magnetic properties of the products were also evaluated by using a superconducting quantum interference device magnetometer (SQUID, MPMS-XL, Quantum Design). Details of this experiments will be described in elsewhere,[37] and this study only uses the results. Briefly, the temperature dependence of the magnetic susceptibilities, χ, was measured at the magnetic field 10 kOe. The Curie−Weiss (CW) temperature, Θ, and the Curie constant, C, were calculated from the experimental data between 50 and 300 K using CW law, $\chi = C/(T-\Theta)$. The effective moment, p_{eff}, was calculated as the equation, $p_{eff} = (3k_B/N_A\mu_B \times C)^{1/2}$, where k_B, N_A, and μ_B are Boltzmann constant, Avogadro number, and Bohr magneton, respectively. Thus, theoretical Curie constant is calculated from the effective moments ($p_{eff\text{-}cal}$) with the equation, $p_{eff\text{-}cal} = g \times (S(S+1))^{1/2}$, where g and S are g-factor and the spin quantum number, S, of Co^{2+} ion, respectively. The g-factor value was presumed as 2.35,[20,30]

and the S was fixed as $S = 3/2$ and $S = 1/2$ for Co^{2+} ion at the T_d site and for that at the O_h site, respectively. Then, the $p_{eff\text{-}cal}$ of $CoAl_2O_4$ was calculated using the equation, $p_{eff\text{-}cal} = [\alpha(p_{eff}O_h)^2 + (1-\alpha)(p_{eff}T_d)^2]^{1/2}$, where α, $p_{eff}O_h$, and $p_{eff}T_d$ are inversion parameter mentioned above, the $p_{eff\text{-}cal}$ of Co^{2+} ion at the O_h site and that at the T_d site, respectively. We used this simulated C in order to compare the experimental result.

Results and discussion

Figure 1(a) shows the XRD patterns of the product $CoAl_2O_4$ ($x = 0$) sample as the typical data. The sample is a single phase of $CoAl_2O_4$ with the spinel structure (the unit cell is cubic structure of the space group $Fd3m$). All samples show the quite similar XRD pattern (see Figure 2), hence we regarded all $(Co_{1-x}Zn_x)Al_2O_4$ products as the single phases of the spinel oxide. Figure 1(b) shows the 311 peaks of XRD patterns for all samples (see the footnote explaining the colouring rule of the sample data for various x of $(Co_{1-x}Zn_x)Al_2O_4$ composition). Here, the intensities were normalized and the peak positions were shifted in order to compare the full width of the half maximum (FWHM) of these peaks. This figure indicates that the effect of Zn^{2+} substitution on the FWHM is quite small for $(Co_{1-x}Zn_x)Al_2O_4$ samples. It means that the remarkable differences are not observed for this sample series with respect to their crystallinity and/or the particle size. The sample of $x = 0.7$ looks slightly wide FWHM, but it is judged as the negligible difference. The right-side figure of Figure 2 focuses on the 440 peak as the high angle peak against d value, and it apparently indicates the change in the lattice constant. Interestingly, dependence of the lattice constant on x has two trends, and the mutational point seems to exist around $x \approx 0.55$ (see the drawn line on the figure). Figure 3 plots the relationship between x and the lattice constant calculated from several peaks at high angle region of $2\theta > 45^o$. The absolute values of the lattice constant in this study were almost the same level with that in the previous report for this sample series.[29] The trend-change mentioned above is obviously confirmed, and the mutational point looks about $x \approx 0.5$. As the one of the reason, this trend-change

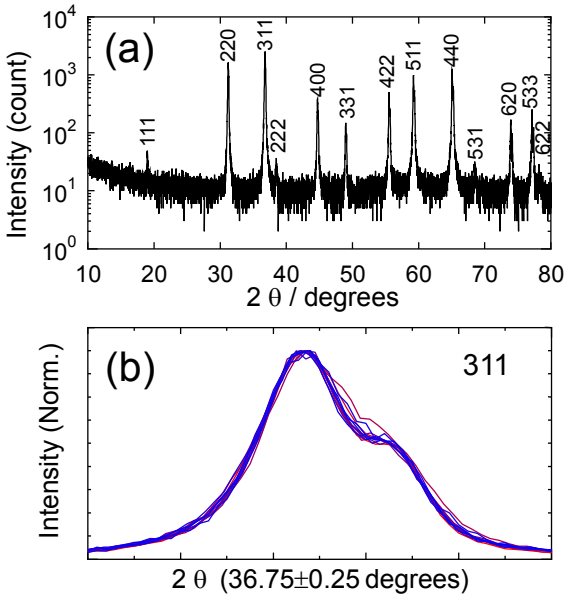

Fig. 1 (a) Indexed XRD pattern of the $CoAl_2O_4$ as the typical product in this study. The vertical axis is set as logarithm scale. (b) Main peaks indexed as 311 in the XRD patterns of all $(Co_{1-x}Zn_x)Al_2O_4$ samples for comparing the FWHM. †

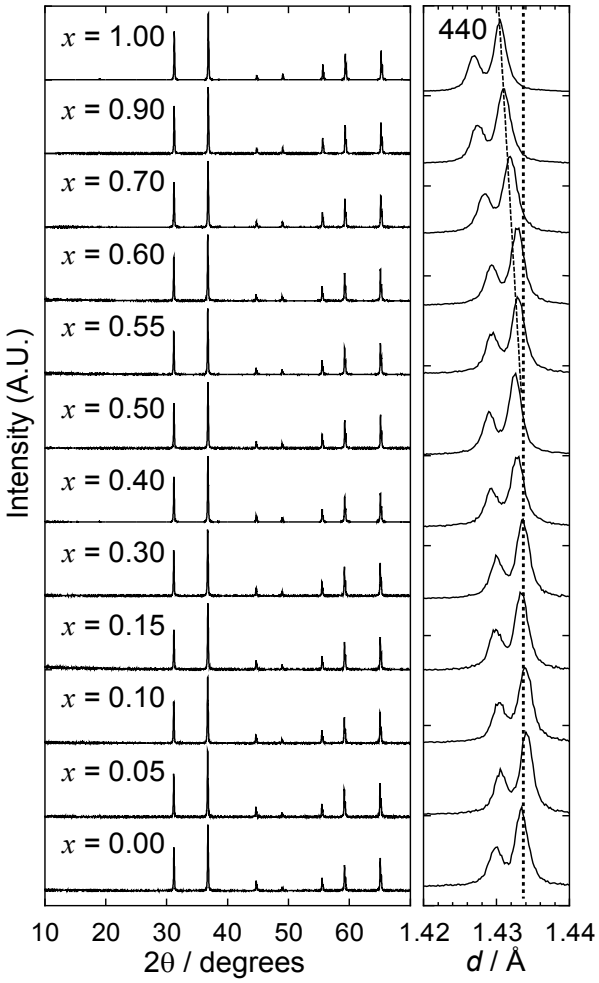

Fig. 2 All XRD patterns of $(Co_{1-x}Zn_x)Al_2O_4$ samples prepared in this study. The right side figure focuses 440 peak around 65° of 2θ plot of the left side figure, and this figure plots against d spacing.

appears associated with the inversion parameter. Thus, Figure 3 also plots the relationship between α and x for the samples of $(Co_{1-x-\alpha}Zn_x)(Al_{2-\alpha}Co_\alpha)O_4$ composition. The inversion parameters of this sample series were relatively smaller (less than 10 %) than previous reports (this value often over 20 %).[22-24] These small α values are not only due to the Zn^{2+} substitution but also to the sintering condition, because that of $CoAl_2O_4$ is also relatively small. The α value is decreased by Zn^{2+} substitution and becomes smaller than 0.01 in case of $Zn_{1-\alpha}(Al_{2-\alpha}Zn_\alpha)O_4$ sample ($x = 1.0$). Both the site exchange and the Zn^{2+} substitution decrease the lattice constant of $(Co_{1-x}Zn_x)Al_2O_4$, then their each contribution to its shrinkage are different and depending on the x. However, we judged that the origin of this trend change is fundamental difference in the crystallographic and the electronic structure between $CoAl_2O_4$ and $ZnAl_2O_4$ rather than the influence of the site exchange phenomena. The ionic radiuses of $Co^{2+}(T_d)$, $Zn^{2+}(T_d)$ and Al^{3+} (O_h) are 0.56, 0.60 and 0.54 (Å) respectively. Thus, Zn^{2+} substitution on Co^{2+} site is considered to introduce some frustration in the basic structure of $CoAl_2O_4$. Then, $x \approx 0.5$ was speculated as some borderline, where the basic structure was changed from $CoAl_2O_4$ to $ZnAl_2O_4$. Probably, we can observe this phenomenon, since the α value of our samples has small.

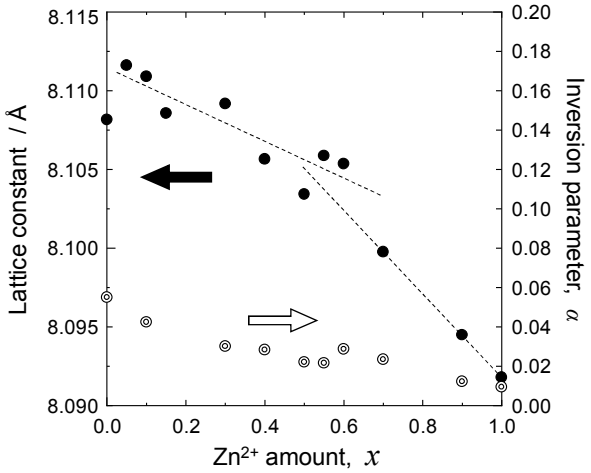

Fig. 3 Dependence of the lattice constant and the inversion parameter, α, on the x of $(Co_{1-x-a}Zn_x)(Al_{2-a}Co_a)O_4$ samples.

The local structural change due to the Zn^{2+} substitution is considered affecting the RS of $(Co_{1-x}Zn_x)Al_2O_4$ samples. Figure 4 is the results of the RS for this sample series, and the typical peaks of $CoAl_2O_4$ are seen at around 200, 416, 520 and 650 cm^{-1}. According to the previous reports for the spinel oxides,[40-42] these Raman bands of spinel structure around 200, 416, 520 and 650 cm^{-1} were assigned as the bending vibration mode of Co-O bond (F_{2g}), vibration mode of Al-O bond, stretching vibration mode of both Co-O and Al-O bonds (F_{2g}) and vibration mode of Co-O bond (A_{1g}), respectively. The intensity of the main peak around 200 cm^{-1} become to be small for the sample with high x value, and this Raman band was not observed in the RS of $ZnAl_2O_4$ sample ($x = 1$). It is contrast with the Raman band around 650 cm^{-1}.

The peak position of RS depends on the local structure of the material, thus it is checked for confirming the trends shown in Figure 2 and 3 for the XRD patterns. Figure 5 plots the peak position of Raman bands around 200 cm^{-1} and 416 cm^{-1} as the typical data. We can find the trend-change like Figure 3 about the lattice constant. The gradient of the peak shift against x looks changing at $x \approx 0.5$ in case of the main peak of 200 cm^{-1}. However, peak position of the band around 416 cm^{-1} looks monotonically shifting to the high wavenumber side with corresponding to the Zn^{2+} substitution level. This is reasonable trend, and thus we concluded that the shrinkage of the lattice constant of $(Co_{1-x}Zn_x)Al_2O_4$ by Zn^{2+} substitution mainly attribute to the change in Co-O bond length rather than that of Al-O bond. On the other hands, the special feature is observed for the Raman band around 200 cm^{-1}. Here, the sideband peaks appear and increase with Zn^{2+} substitution proceeds. This is interesting phenomena found in this study, since these sideband peaks appeared in $(Co_{1-x}Zn_x)Al_2O_4$ series are thought to be the first detection for the spinel oxide. Our background experiments performed shows that we could not find these clear sideband peaks for $(Co_{1-x}Mg_x)Al_2O_4$ series although the similar peaks were weakly observed for the sample with high x value. We checked the RS of the impurity phases considered in this study; like CoO, ZnO, Al_2O_3 and Co_3O_4, but they do not have the Raman band for this wavenumber region. Therefore, they are considered as the inherent spectroscopic signature of $(Co_{1-x}Zn_x)Al_2O_4$ series. Figure 6 focuses these sideband peaks normalized by the intensity of the main peak around 200 cm^{-1}. Interestingly, peak positions of the sideband peaks looks unchanged corresponding to the Zn^{2+} substitution proceeds, it is in contrast to the systematic shift of the main peak position. We speculated that the sideband

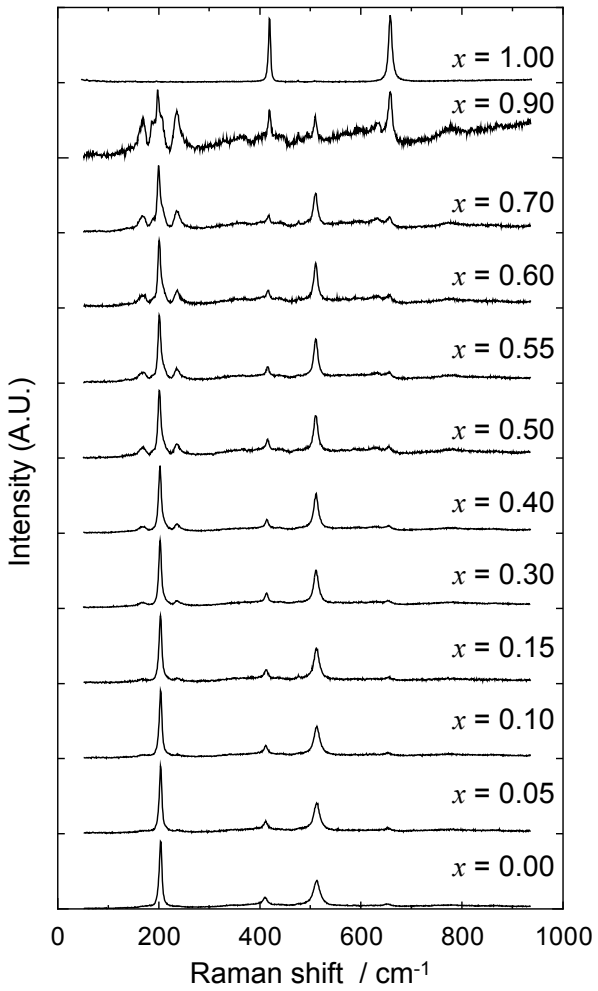

Fig. 4 All Raman spectra measured for $(Co_{1-x}Zn_x)Al_2O_4$ samples prepared in this study.

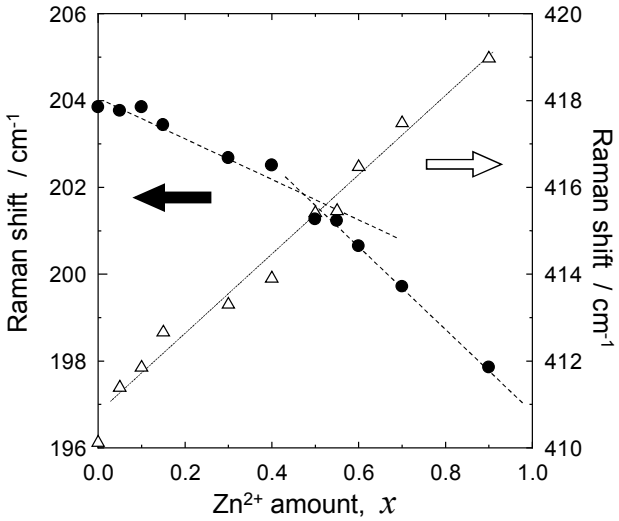

Fig. 5 Peak positions of the Raman bands around 200 cm^{-1} and 416 cm^{-1} of the Raman shift for all samples. The data are plotted against x of the $(Co_{1-x}Zn_x)Al_2O_4$ composition.

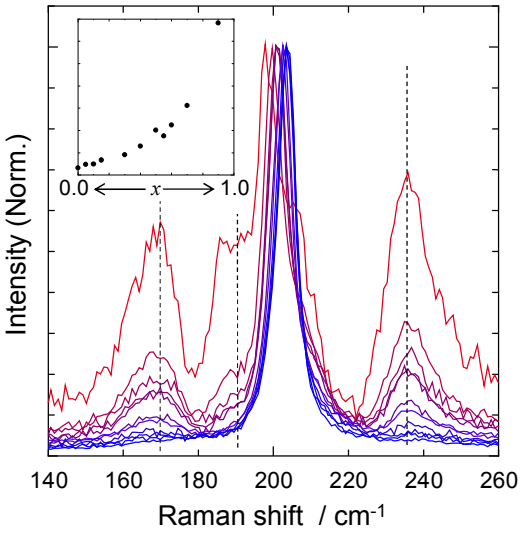

Fig. 6 Normalized main peak of the Raman band around 200 cm^{-1} measured for all $(Co_{1-x}Zn_x)Al_2O_4$ samples. Inserted figure shows the x dependence of the normalized intensity of the sideband peaks around 236 cm^{-1}. †

peaks relate to some energy level created by Zn^{2+} substitution for T_d site of $CoAl_2O_4$. Moreover, the relative intensities of the sideband peaks looks becoming prominent for the sample of $x \geq 0.5$ (see the inserted figure plotting it against the x). This non-linear trend seems to relate to the trend-change observed in Figure 3(XRD) and 5(RS). Therefore, we considered that the origin of the trend-change is not only the site change phenomenon, but also the local electronic structural change. However, the origin of both sideband peaks and the trend-changes have not been cleared, yet. The differences in the wavenumber of these sidebands from the main peak are about 40 cm^{-1} (≈ 5 meV). On the other, these peaks are calculated as ≈ 21 and 29 meV against incident light of 532 nm. These values inspire us some possibility. We felt that the systematic evaluation using thin film or single crystal enables us to clarify these peaks. This is an interesting phenomenon from the viewpoint of physics, so that further investigation is in progress now.

Here, we want to suggest the utilization of these sideband peaks as the indicator to discuss the substitution level of Zn^{2+} for $(Co_{1-x}Zn_x)Al_2O_4$. This substitution level is difficult to guess from the lattice constant. Because, lattice constant is not clear indicator especially for the sample of $x < 0.7$ (see Figure 3), since this value closes and scatters. In contrast, intensities of the sideband systematically changed with corresponding to the Zn^{2+} substitution proceeds, and the discriminable range looks to be $x \geq 0.1$. Thus, RS measurement are thought to be key characterization for discussing the effect of Zn^{2+} substitution on the properties of $(Co_{1-x}Zn_x)Al_2O_4$. Note that, the shoulder peak is also observed around 190 cm^{-1}. This is considered to associate with the partial substitution of A site in the spinel AB_2O_4 oxide by the other cation, because it is clearly observed for the RS of $(Co_{1-x}Mg_x)Al_2O_4$ series.

Above discussion for the sideband peak implies the local change in the electronic structure of the $CoAl_2O_4$ by Zn^{2+} substitution. Thus, Figure 7 plots the relative change in the valence values of Co^{2+}, Al^{3+} and O^{2-} ions determined from BVS calculation for the $(Co_{1-x}Zn_x)Al_2O_4$ samples. It indicates that the covalent character of each bond is reduced by Zn^{2+} substitution. That is, Zn^{2+} substitution is considered to change uniquely the local electronic state of $CoAl_2O_4$ (meaning charge distribution in the unit cell). This is explained with the difference between the electronegativities of Co^{2+} (1.88) and Zn^{2+} (1.65). This change in the charge distribution is thought contributing to the appearance of the sideband peaks in RS of $(Co_{1-x}Zn_x)Al_2O_4$ system. Note that, the BVS values in Figure 7 looks scattering from the linear trend in the case for $x \leq 0.5$. Present study regards it relating to the difficulty of the accurate Rietveld refinement for the sample with high inversion parameter, therefore we excluded this point from the discussion. However, $x \approx 0.5$ looks the border for the something; hence more precise analysis for the Rietveld refinement is in progress now. [37]

In general, RS and FT-IR spectra give us complementary information to discuss the local structural change in the material. Therefore, we performed FT-IR measurement. The result is shown in Figure 8 with plotting the relative intensity against main peak around 670 cm^{-1}. The bands of the metal–oxygen bonds in spinel structure appear at the region between 1000 and 400 cm^{-1}. [24,32,33,43-49] The

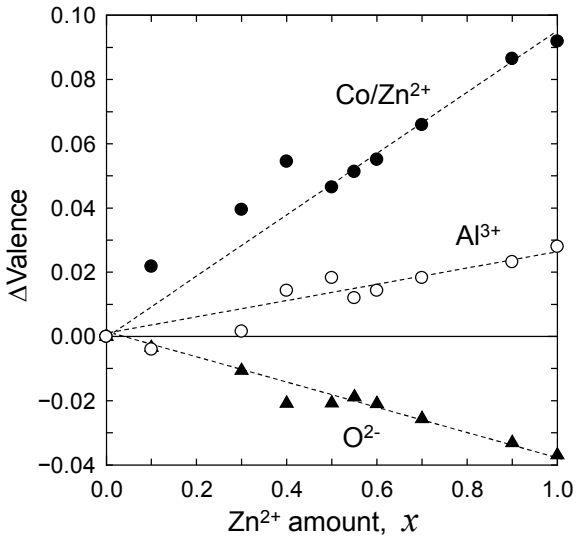

Fig. 7 Results of BVS calculations using the refinement data of the Rietveld analysis performed for all XRD data of $(Co_{1-x}Zn_x)Al_2O_4$ samples.

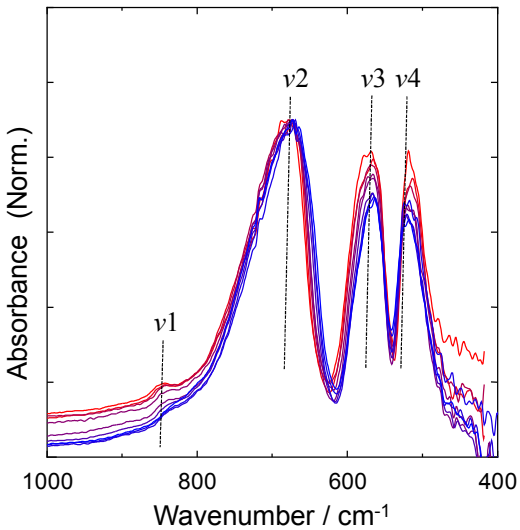

Fig. 8 FT-IR spectra of $(Co_{1-x}Zn_x)Al_2O_4$ samples plotted against wavenumber. †

distinctive bands are shown around 840 (ν1), 670 (ν2: F_{1u}), 570 (ν3: F_{1u}) and 520 (ν4: F_{2g}) cm^{-1}.[24,44] These bands are typical signal of the FT-IR spectra for $CoAl_2O_4$. Then, the ν2 and ν3 bands are assigned as the Co-O vibration modes.[41] Here, the relative peak intensities of ν3 and ν4 looks systematically increasing with Zn^{2+} substitution proceeds. However, it is considered to be affected by the background line strongly depending on the measurement condition using KBr pellet. Thus, we excluded this trend from the discussion. The peak position of all bands looks unchanged by the Zn^{2+} substitution. The change of the lattice constant is quite small (less than 1%), thus there is not the remarkable change in the energy of infrared activity mode of this sample series probably. However, we slightly felt that the shoulder band of ν1 shifted to high wavenumber side. We speculated that this band also relates to the Co-O bond. On the other hand, systematic change seems appeared in the peak width of ν2, ν3 and ν4 bands. They show asymmetric change against Zn^{2+} substitution. According to the previous report performing the peak analysis of FT-IR spectra for $CoAl_2O_4$, observed these bands split into transverse optical mode and longitudinal one, and these splitting supplies a criterion for the ionic character.[44] The bands of longitudinal optical mode of ν2 and ν3 are around 760 and 600 cm^{-1} respectively, and these region of our data looks fatting corresponding to Zn^{2+} substitution proceeds. Therefore, Figure 8 seems indicating that the Zn^{2+} substitution enhance the ionicity of Co-O bond of $CoAl_2O_4$. This is consistent with the result of BVS calculation in Figure 7.

As the next step, we measured the UV-VIS spectra of $(Co_{1-x}Zn_x)Al_2O_4$ samples in order to evaluate the visible light absorption of them. Because, the colors of the product samples depend on the x value and they were systematically changed from blue of x = 0 to white of x = 1. Figure 9 shows the results for the region of the visible light (413 ~ 885 nm). The main absorption bands around 1.8 ~ 2.5 eV seems to become sharp corresponding to Zn^{2+} substitution proceeds, and thus the low energy side of the absorption bands looks shifting to high energy side corresponding to the Zn^{2+} substitution proceeds. According to the previous study,[29] main absorption bands around 1.8 ~ 2.5 eV attribute to the five bands. Here, the quadruplet $^4T_1(^4P)$ transition overlaps four doublet transitions originated from the ^2G term: ^2E, $^2T_1$, $^2T_2$, and $^2A_1$. The distinguishable bands of $^4T_1$ transition are shown around 1.96 eV and 2.08 eV respectively, and the first one strongly mixed with the ^2E and/or $^2T_1$ states. A third

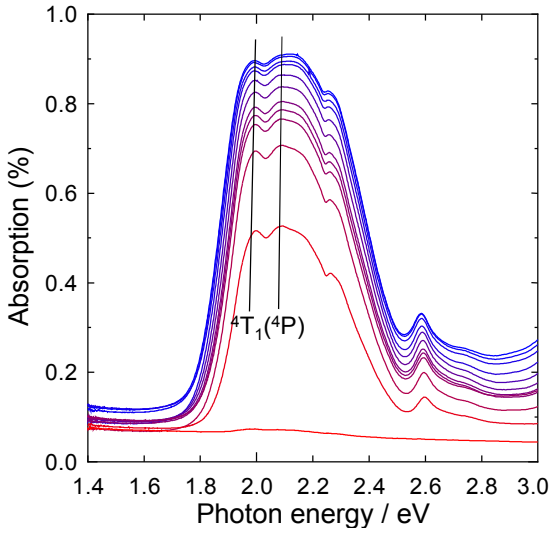

Fig. 9 Results of UV-VIS measurement for all $(Co_{1-x}Zn_x)Al_2O_4$ samples. Here, the data are focused on the region of visible light and plotted against the photon energy. †

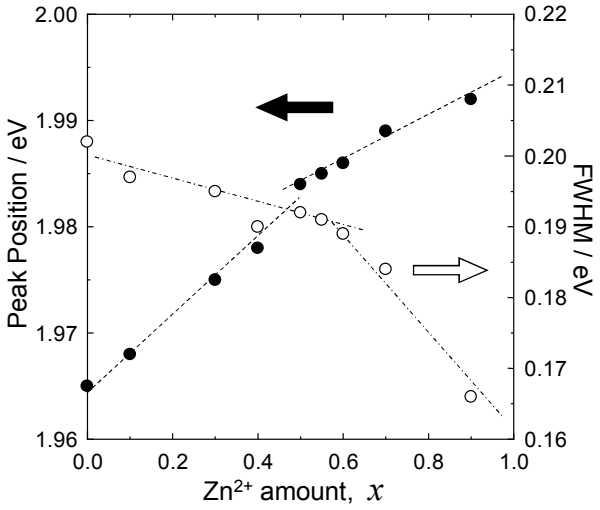

Fig. 10 The peak position and the FWHM of $^4T_1(^4P)$ transition in the *d-d* transition observed in the UV-VIS spectra. They are plotted against x of $(Co_{1-x}Zn_x)Al_2O_4$ samples.

band at about 2.25 eV is assigned as the $^2A_1$ and $^2T_2$ spin-allowed transitions, whose anomalous intensity stems from vibronic effects in the 2.11 ~ 2.29 eV interval. Peak separation of these overlapped bands is quite delicate analysis. So, we simply analyze the left-side peak by fitting this area using Gaussian function, since only this left-side is not affected by the overlapping with the another peak.[29] Figure 10 plots the determined peak position and the FWHM of this $^4T_1(^4P)$ transition. The peak shift from x = 0.0 to x = 1.0 is about 0.025 eV, although the low energy side of the absorption bands shown in Figure 9 looks shifting about 0.1 eV. This is consistent with that the peak positions relating to $^4T_1$ transition look almost the same (see the line in Figure 9). It means that the change in the low energy side of the absorption bands shown in Figure 9 (≈ 0.1 eV) is mainly attributing to the change in the FWHM of this peak rather than the shift (≈ 0.025 eV) of the transition energy of this left-side band. Interesting point is that both the peak position and the FWHM show the trend-change similar with the data of Figure 3(XRD) and 5(RS). This consistency is considered as the reasonable trends. Because, the transition energy of this band mainly depends on the Co-O bond length, and the FWHM mainly depends on the adiabatic potential curve of this bond.[50,51]

Remarkable point is that the trend-change around $x \approx 0.5$ is identified from the data of XRD, RS and UV-VIS. It means that this tend-change is due to the change in the lattice constant mainly depends on the Co/Zn-O distance. The difference between the sample of $x \leq 0.5$ and that of $x \geq 0.5$ is not cleared, but this local crystallographic change should affect the electronic structure of this spinel oxide. Non-linear enhancement in the relative intensities of the sideband peaks in RS is considered relating to this electronic structural change. About this difference in the electronic structure between $x \leq 0.5$ and $x \geq 0.5$, some unique characteristics were found in its spectroscopic behaviour. Next, we introduce them.

The intensity of the main absorption bands in UV-VIS spectra for the region of 1.8 ~ 2.5 eV becomes to be small with increasing the Zn^{2+} substitution level (see Figure 9). This is reasonable result, because the amount of Co^{2+} is the origin of this absorption bands (*d-d* transition). Figure 11 plots the integrated intensity of this main peak plotted against x in order to check the relationship between x and the blueness of this sample series. The blueness of $(Co_{1-}$

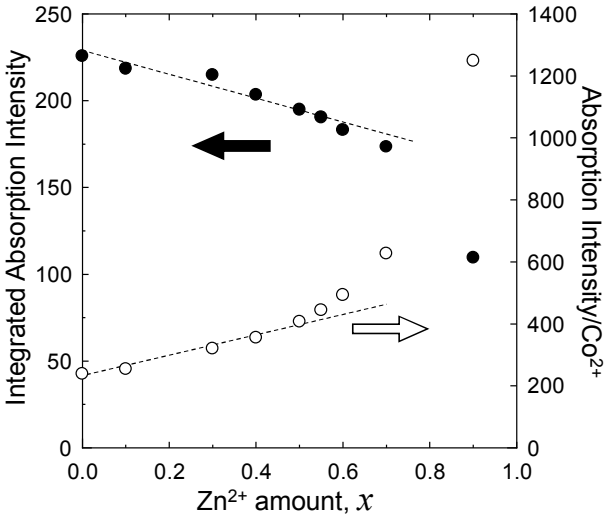

Fig. 11 Zn^{2+} amount, x, dependence of the integrated absolute absorption intensity and the normalized value by the Co amount, 1-x, of the *d-d* transition in a photon energy range between 1.4 ~ 2.8 eV.

$_x$Zn$_x$)Al$_2$O$_4$ should depend on the amount of Co^{2+}, therefore constant degradation is expected as the reasonable trend. However, this degradation curve of the blueness against x seems to become steep for the region of $x \geq 0.7$. This trend looks similar with the data shown in elsewhere.[50] Figure 11 indicates at least that the borderline to keep the blueness of $CoAl_2O_4$ is about 70 % for the Zn^{2+} substitution to the Co^{2+} site. This high value is thought to be favorable for the usage of $(Co_{1-x}Zn_x)Al_2O_4$ series as the pigment, since the precise controlling of the cation composition less than 20% is sometimes difficult for fabricating the nanoparticles or thin film or single crystal of this material. Here, we found the data spotlighting the sample of $x \geq 0.5$. Figure 11 also plots the intensity value divided by x. This value simulating the absorption intensity of each Co^{2+} in $(Co_{1-x}Zn_x)Al_2O_4$ samples. For this calculation, we took into account for the influence of the site change phenomena. It is not constant for the range of $0 \leq x < 1$. Non-linearly increasing is observed in this figure, and the intensity of each Co^{2+} become to be prominently stronger for the sample of $x \geq 0.5$. This trend is good agreement with that in inserted graph of Figure 6. This result is considered as the valuable information for the investigation of the optical property and/or the catalytic function of the spinel oxide.

Furthermore, the similar trend is identified from the other experiments. Here, the fluorescence property was observed for our $(Co_{1-x}Zn_x)Al_2O_4$ samples as the novel functional property. Figure 12 shows the RS measured for high Raman-shift-region around 3300 cm^{-1}. This figure plotted the normalized intensity by the maximum against the energy of the detected light. Apparently, high intensity peak was seen in this figure. Here, small peaks around 2.3 eV is the typical RS shown in Figure 4. The strong peaks around 1.85 ~ 1.9 eV are broader and the intensities of them are 1 order larger than the typical RS. Then, the energy corresponds to the absorption edge discussed for UV-VIS spectra shown in Figure 9. The edges of high energy peak in Figure 12 shift to high energy side corresponding to the Zn^{2+} substitution proceeds. Moreover, the peak width looks becoming sharp by Zn^{2+} substitution. These trends seem all corresponds with the UV-VIS data shown in Figure 9. Therefore, these high energy peaks are considered as the fluorescence of $(Co_{1-x}Zn_x)Al_2O_4$ samples. The origin is considered relating to the absorption light of the *d-d* transitions. The peak shapes seems essentially the same for all $(Co_{1-x}Zn_x)Al_2O_4$ except for $ZnAl_2O_4$ of $x = 1$. It seems that the fluorescence mechanisms are essentially the same for these samples. Meanwhile, we measured the fluorescence of the $ZnAl_2O_4$, interestingly. This sample is white color without the light absorption due to the *d-d* transition. Therefore peak shape is apparently different with that of the other samples, so that it is further interesting. Note that, some of works reports the photoluminescence of $(Co_{1-x}Zn_x)Al_2O_4$ samples, but they often misunderstand the double wave or this kind of waves (detected owing to the measurement condition). On the other hand, our data shows systematic change in the peak position and in the sharpness against x of $(Co_{1-x}Zn_x)$ Al_2O_4 composition, so that we believe it intrinsic fluorescence properties of this sample series. Considering about the energy of the excitation light (532 nm = 2.33 eV), $^2T_1(^2G)$ transition[29] is at least excluded from the discussion about the origin of this fluorescence phenomena. This assignment requires further investigation.

Figure 13 plots the absolute values of the maximum intensity of

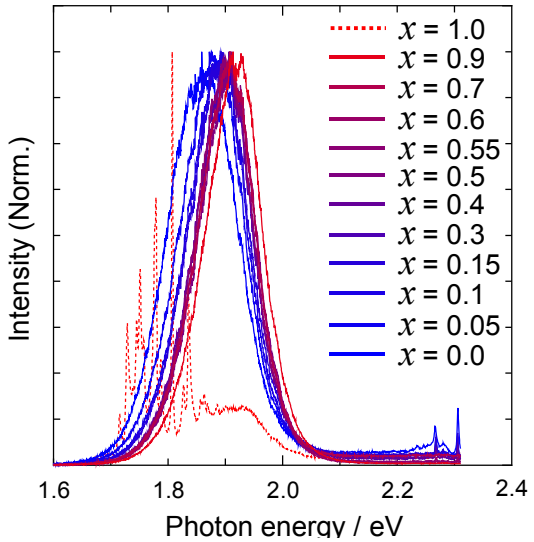

Fig. 12 Raman spectra of $(Co_{1-x}Zn_x)Al_2O_4$ samples plotted against the photon energy of the detected light for the high Raman shift region. †

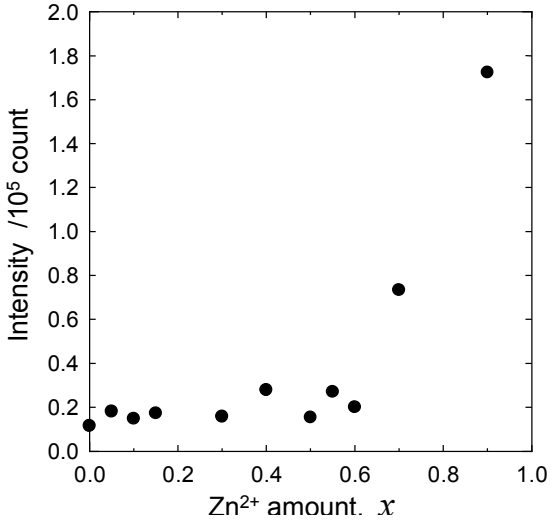

Fig. 13 Absolute intensity of the fluorescent peak observed for the RS of the high Raman shift region. The data are plotted against x of $(Co_{1-x}Zn_x)Al_2O_4$ composition.

the fluorescence peak of $(Co_{1-x}Zn_x)Al_2O_4$ samples measured at the same condition. Interestingly, this peak intensity increases drastically at high Zn^{2+} substitution region of $x > 0.7$. This is interesting trend, because it reminds us the phenomena discussed in Figure 6(RS) and Figure 11(UV-VIS). This trend itself is observed not only for the $(Co_{1-x}Zn_x)Al_2O_4$ series but also for the $(Co_{1-x}Mg_x)Al_2O_4$ series. Therefore, we thought that the fluorescence mechanism of this spinel oxide does not directly concern with the sideband peaks shown in Figure 5(RS). However, we experimentally found that the maximum intensity of $(Co_{0.1}Zn_{0.9})Al_2O_4$ is much higher than that of $(Co_{0.1}Mg_{0.9})Al_2O_4$. So, we consider that some physical phenomenon leading the sideband peak of RS has a probability contributing to the enhancement in the fluorescence light of the spinel oxide. This result seems interesting for the investigation of the luminescence material with spinel structure like $CaAl_2O_4$ and it's related materials.

The fluorescence property identified in this study is considered as the novel functional property of $(Co_{1-x}Zn_x)Al_2O_4$ series. However, more precise discussion requires the returning to the investigation about the sample preparation. Because, the intensity of this fluorescence was not high, hence we could not observe the same result from the experiments using PL spectroscopy. Figure 14 shows the result for $CoAl_2O_4$ with including the data of RS in Figure 12. We could find the RS indicated as the dash line in Figure 14 for both results of PL spectroscopy and that of RS. However, fluorescence peak observed in RS was not observed in PL data. This data indicates at least that the high intensity peak shown in Figure 12 does not originate in the Raman band of this spinel oxide. The difference between these two measurements is the intensity of the incident light. The semiconductor laser used for the incident light of RS is considered working as the excitation light source, although the intensity of the diffracted ray from the xenon light (used for the PL) is not enough for the same usage. We speculated from these data that the origin of this fluorescence phenomenon is not the major area in the sample. However, we also speculated from the consideration about the XRD patterns in Figure 2 and the correspondence relationship between Figure 9 (UV-VIS) and Figure 12 (fluorescence in RS) that the minor phase is not the impurity phase. Therefore, we speculated the possibilities about the existence of the local inhomogeneous area and/or that of the some special structure of $(Co_{1-x}Zn_x)Al_2O_4$.

From this reason, the temperature dependence of the susceptibility of $(Co_{1-x}Zn_x)Al_2O_4$ samples is measured in order to discuss the inhomogeneity in this material. The data are described in elsewhere.[30] Here, the calculated CW temperature and the Curie constant were plotted against x of the substitution level in Figure 15. It looks that both values change linearly corresponding to the Zn^{2+} substitution level. Inserted solid line in this figure is result of the simulation about the x dependence of Θ for $(Co_{1-x}Zn_x)Al_2O_4$. They mean that the correlation between Co^{2+} cations is consistently

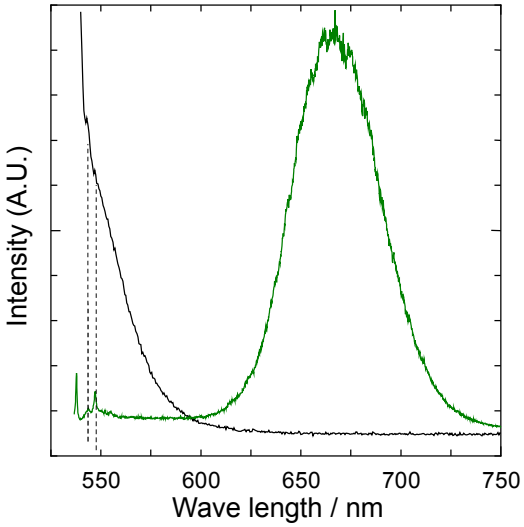

Fig. 14 Comparison of the PL spectroscopy and the RS of high Raman shift region for $CoAl_2O_4$ sample. The data are plotted against wave length of the detected light.

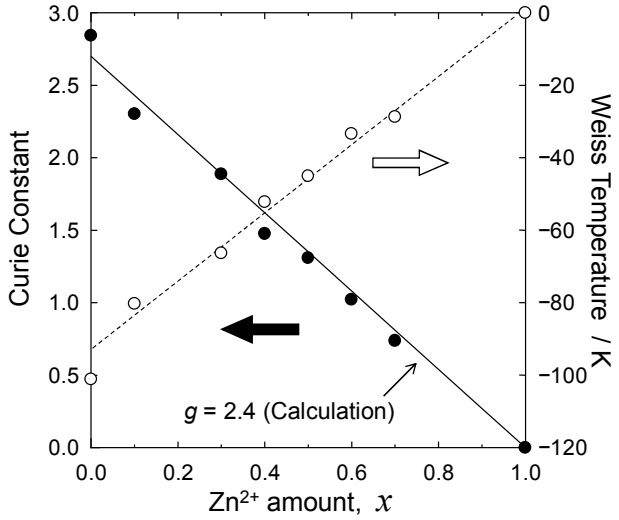

Fig. 15 The Currie constant and the Weiss temperature of all samples. The data are plotted against x of $(Co_{1-x}Zn_x)Al_2O_4$ composition.

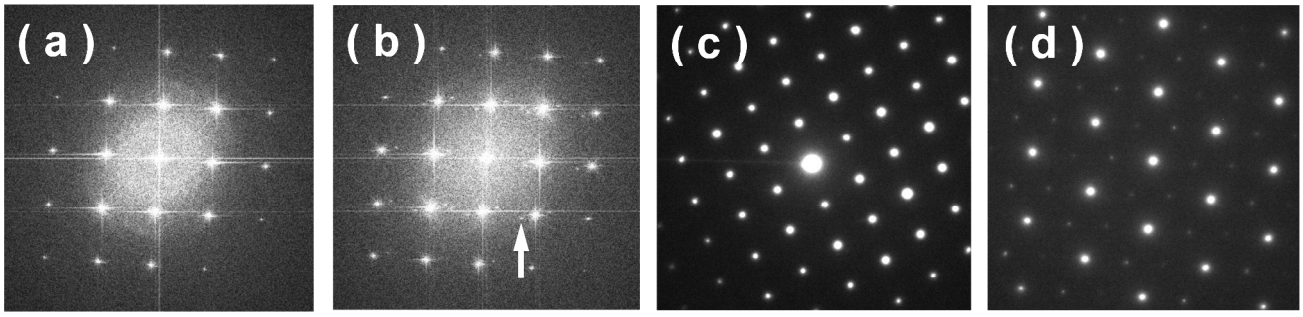

Figure 16 TEM diffraction patterns of <100> direction observed in the $(Co_{0.45}Zn_{0.55})Al_2O_4$ sample (a)(b) and those of <111> direction observed in the $(Co_{0.1}Zn_{0.9})Al_2O_4$ sample (c)(d).

reduced corresponding to the decline of Co^{2+} by Zn^{2+} substitution. That is, inhomogeneity of the Zn^{2+} substitution or existence of high Co^{2+} area is not implied from Figure 15.

On the other hand, result of TEM observation implies the existence of the unknown area in (Co, Zn)Al_2O_4 sample. Figure 16 shows the electron diffraction (ED) images observed for the $(Co_{0.45}Zn_{0.55})Al_2O_4$ sample. The crystal structure of $CoAl_2O_4$ is normal spinel of cubic system, thus this image is observed from <100> direction. Almost area of the $(Co_{0.45}Zn_{0.55})Al_2O_4$ grain shows the ED images as shown in Figure 16(a) indicating the simple cubic structure of the spinel oxide, whereas we sometimes observed the satellite spot in the image (see Figure 16(b)). Moreover, we observed ED images shown in Figure 16(d) for the $(Co_{0.1}Zn_{0.9})Al_2O_4$ sample. This image is observed from <111> direction, and the spot indicating super structure is observed. This is different with the normal ED image of <111> direction (see Figure 16(c)). We could not find the difference between the high resolution images of these specific area and that of the normal area. Thus, these phases are considered as the local area with unique structure having some cation ordering and/or anion deficient. Based on our experience observed for some $(Co_{1-x}Zn_x)Al_2O_4$ including the end member, the structure like Figure 16(b) was found in the sample of $x \approx 0.5$, and that like Figure 16(d) was found in the sample of $x \approx 0.9$. Thus, the former is expected relating to the trend-change in the lattice constant at around $x \approx 0.5$, and the later is expected as the origin of the fluorescence phenomenon. However, finding process of these phases is not easy now, because these specific areas are thought to be minor phases in the observed area. In addition, phase inhomogeneity was not implied from Figure 1(b). Therefore, leading the conclusion that the fluorescence phenomenon found in this study originates in these minor phases is quite difficult for the present study. We believe that the precise discussion become to be possible by realizing the single-phase preparation of $(Co_{1-x}Zn_x)Al_2O_4$ sample with these specific structure. It is also expected to open up the discovery of the novel functional property in spinel materials,[51] hence further investigation is required.

Conclusions

This work investigates the spectroscopic property of $(Co_{1-x}Zn_x)Al_2O_4$ for the wide range x of $0 \le x \le 1$. The samples were sintered at high temperature of 1300 °C and slowly cooled for 24 hours in order to minimize the some deficiencies in the structure. Thus, inversion parameters of the samples were relatively lower than that of other reports.

The crystallographic and the spectroscopic evaluations were performed for this $(Co_{1-x}Zn_x)Al_2O_4$ by using XRD, Raman spectroscopy, FT-IR and UV-VIS. The results reveals that the Zn^{2+} substitution mainly changes the Co-O bond of the $CoAl_2O_4$, thus the lattice constant of $(Co_{1-x}Zn_x)Al_2O_4$ systematically varied corresponding to the substitution level. Here, the systematic change in the lattice constant is not monotonic, and the trend-change is identified at around $x \approx 0.5$ in the plots for the x dependences of some properties relating to the lattice constant. The reason for this trend-change in the lattice constant is probably due to the structural frustration between $CoAl_2O_4$ and $ZnAl_2O_4$. This local crystallographic change should affect the electronic structure of this spinel oxide. The results of BVS and FT-IR indicate that the Zn^{2+} substitution enhance the iconicity of each bond of $CoAl_2O_4$. The remarkable point is that this electronic structural change influences some spectroscopic characteristics of this material, and they become to be prominent for the sample of $x \ge 0.5$. That is, relative intensities of the sideband peaks, efficiency in the absorption intensity for the visible light of Co^{2+} and the intensity of the fluorescence peak in $(Co_{1-x}Zn_x)Al_2O_4$ is non-linearly enhanced by Zn^{2+} substitution proceeds, and they prominently become to be strong for the sample of $x \ge 0.5$.

This study found four novel and/or anomalous properties in $(Co_{1-x}Zn_x)Al_2O_4$ samples. (1) The one is the spectroscopic phenomena mentioned above for the sample of $x \ge 0.5$. These results are considered as the valuable information for the investigation of the optical property and/or the catalytic function of the spinel oxide. On the other hand, (2) the sideband peaks appear near the main peak of the RS are also considered as the inherent spectroscopic signature in the series of $CoAl_2O_4$ with Zn^{2+} substitution. We speculated that the sideband peaks relate to some energy level created by Zn^{2+} substitution for T_d site of $CoAl_2O_4$, and that the energy is similar with the impurity level in the band gap of the semiconductor. This is interesting phenomena from the viewpoint of the material science and the physics. Moreover, these sideband peaks are considered useful indicator for discussing the substitution level of Zn^{2+} for $(Co_{1-x}Zn_x)Al_2O_4$. Because, the peak intensities of these sidebands depended on the Zn^{2+} substitution level, and the resolution looked much better than the estimation from the XRD data. In addition, (3) fluorescence peak observed in the RS, is also quite interesting phenomenon. As the speculation, $(Co_{1-x}Zn_x)Al_2O_4$ sample with the superstructure relates to this phenomenon. We believe that the precise discussion become to be possible by realizing the single-phase preparation of $(Co_{1-x}Zn_x)Al_2O_4$ sample with these specific structure. Furthermore, (4) existence of these phase with unique structure itself is also interesting. It is also expected to open up the discovery of the novel functional property in the spinel materials.[51] This study at least verifies the possibility to fabricating these phase, so that purifying these phases is believed as the challenging future work for tailoring novel functional property in the spinel oxide.

The spinel oxide is widely investigated material. However, spectroscopic evaluation for $(Co_{1-x}Zn_x)Al_2O_4$ in this study could find some interesting characteristics in this material by preparing material with widely and precisely controlled x value. This study focuses on showing these interesting characteristics, and the details are not cleared yet. Now, these characteristics reviewed in this study are believed to become a lot of seeds for the material science and its application for the spinel oxide. Therefore, we suggest further investigation for the $(Co_{1-x}Zn_x)Al_2O_4$; especially for the high x region.

Acknowledgements

We acknowledge the Dr. Isamu Yamada of MANA in National Institute for Materials Science (NIMS) for his technical contribution. His sophisticated technique for the TEM observation images helps this study a lot.

This work was partially supported by a Grant-in-Aid for Scientific Research (A) (KAKENHI) No. 25246013.

Notes and references

[a] National Institute for Materials Science, Sengen 1-2-1, Tsukuba, Ibaraki 305-0047, Japan.

[b] Institute of Multidisciplinary Research of Advanced Materials, Tohoku University, Katahira 2-1-1, Aoba-ku, Sendai 980-8577, Japan.

[c] Department of Applied Chemistry, Faculty of Science and Engineering, Chuo University, Kasuga 1-13-27, Bunkyo-ku 112-8551, Japan.

† This study sometimes use the colour figure, and the colouring rule for the sample data depends on the x of $(Co_{1-x}Zn_x)Al_2O_4$ composition; i.e.

plotting color was selected for the data of $(Co_{1-x}Zn_x)Al_2O_4$ sample to be RGB[255*x*, 0, 255(1-*x*)]. That is, the plotting color is varied from blue (for $CoAl_2O_4$) to red (for $ZnAl_2O_4$). It is corresponding to the Zn^{2+} substitution level, and thus the purple of RGB[128, 0, 128] means the data for $(Co_{0.5}Zn_{0.5})Al_2O_4$ sample.

Electronic Supplementary Information (ESI) available: [details of any supplementary information available should be included here]. See DOI: 10.1039/b000000x/

1. I. B. Bersuker, *Electronic Structure and Properties of Transition Metal Compounds*, John Wiley & Sons, New York, 1996.
2. E. P. Wohlfarth, *Ferromagnetic Materials*: *a handbook on the properties of magnetically ordered substances vol. 3*, Elsevier, New York, 1982.
3. P. A. Cox, *Transition Metal Oxides*, Oxford University, New York, 1992.
4. E. B. Faulkner and R. J. Schwartz, *High Performance Pigments*, Wiley-VCH, Weinheim, 2009.
5. G. Buxbaum and G. Pfaff, G. *Industrial Inorganic Pigments*, Wiley-VCH, Weinheim, 2005.
6. L. D. Kock and D. De Waal, *J. Raman Spectrosc*., 2007, **38**, 1480−1487.
7. H.A. Bethe, *Ann*. *Physik*, 1929, **3**, 133-206.
8. G. Racah, *Phys*. *Review* 1942, **62**, 438-462.
9. Y. Tanabe and S. Sugano, *J. Phys*. *Soc*. *Jap*., 1954, **9**, 753-766.
10. Y. Tanabe and S. Sugano, *J. Phys*. *Soc*. *Jap*., 1954, **9**, 766-779.
11. Y. Tanabe and S. Sugano, *J. Phys*. *Soc*. *Jap*., 1956, **11**, 864-877.
12. L. Ji, S. Tang, H. C. Zeng, J. Lin and K. L. Tan, *Appl*. *Catal*. *A*, 2007, **207**, 247-255.
13. A. Walsh, Y. Yan, M. M. Al-Jassim and S.-H. Wei, *J. Phys*. *Chem*. *C*, 2008, **112**, 12044-12050.
14. A. Walsh, S.-H. Wei, Y. Yan, M. M. Al-Jassim and J. A. Turner, *Phys*. *Rev*. *B*, 2007, **76**, 165119/1-9.
15. K.-S. Ahn, Y. Yan, M.-S. Kang, J.-Y. Kim, S. Shet, H. Wang, J. Turner and M. M. Al-Jassim, *Appl*. *Phys*. *Lett*., 2009, **95**, 022116/1-3.
16. M. Hagiwara, S. Kimura, N. Nishihagi, T. Suzuki, M. Nohara, H. Takagi and K. Kindo, *J. Low Temp*. *Phys*., 2010, **159**, 11-14.
17. T. Suzuki, H. Nagai, M. Nohara and H. Takagi, *J. Phys*. *Cond*. *Mater*., 2007, **19**, 145265/1-5.
18. A. Maljuk, V. Tsurkan, O. Zeharko, A. Cervellino, A. Loidl and D. N. Argyriou, *J. Cryst*. *Growth*, 2009, **311**, 3997-4000.
19. N. Tristan, V. Zestrea, G. Behr, R. Klingeler, B. Büchner, H. A. Krug von Nidda, A. Loidl and V. Tsurkan, *Phys*. *Rev*. *B*, 2008, **77**, 094412/1-10.
20. N. Tristan, J. Hemberger, A. Krimmel, H. A. Krug von Nidda, V. Tsurkan and A. Loidl, *Phys*. *Rev*. *B*, 2005, **72**, 174404/1-9.
21. F. Tielens, M. Calatayud, R. Franco, J.M. Recio, J. Pérez-Ramírez, C. Minot, *J. Phys*. *Chem*. *B*, 2006, **110**, 988-995.
22. H.S.C. O'neill, *Eur*. *J*. *Mineral*., 1994, *6*, 603-609.
23. A. Nakatsuka, Y. Ikeda, Y. Yamasaki, N. Nakayama and T. Mizota, *Solid State Commun*., 2003, **128,** 85-90.
24. M. Taguchi, T. Nakane, K. Hashi, S. Ohki, T. Shimizu, Y. Sakka, A. Matsushita, T. Funazukuri and T. Naka, *Dalton Ttrans*., 2013, **42**, 7167-7176.
25. D. Rangappa, T. Naka, A. Kondo, M. Ishii, T. Kobayashi and T. Adschiri, *J. Am*. *Chem*. *Soc*., 2007, 129, 11061-11066.
26. D. Rangappa, S. Ohara, T. Naka, A. Kondo, M. Ishii and T. Adschiri, *J. Mater*. *Chem*., 2007, 17, 4426-4429.
27. M. Gaudon, A. Apheceixborde, M. Ménétrier, A. Le Nestour and A. Demourgues, *Inorg*. *Chem*., 2009, **48**, 9085-9091.
28. J. Popović, E. Tkalčec, B. Grželeta, S. Kurajica and B. Rakvin, *Am*. *Mineral*., 2009, **94**, 771-776.
29. M. Ardit, G. Cruciani and M. Dondi, *Am*. *Mineral*., 2012, **97**, 1394-1401.
30. T. Naka *et al*. in preparation
31. K. Hanashima, Y. Kodama, D. Akahoshi, C. Kanadani and T. Saito, *J. Phys*. *Soc*. *Jpn*., 2013, 82, 024702/1-7.
32. K. Sato, T. Naka, T. Nakane, D. Rangappa, S. Takami, S. Ohara and T. Adschiri, *J. Mag*. *Mag*. *Mater*., 2014, **350**, 161-166.
33. F. Mayer, R. Hempelmann, S. Mathur and M. Veith, *J. Mater*. *Chem*., 1999, **9**, 1755-1763.
34. M. Zayat and D. Levy, *Chem*. *Mater*., 2000, **12**, 2763-2769.
35. N. El Habra, L. Crociani, C. Sada, P. Zanella, M. Casarin, G. Rossetto, G Carta and G. Paolucci, *Chem*. *Mater*., 2007, **19**, 3381-3386.
36. H.M. Rietveld, *J. Appl. Crystallor.* 1969, **2**, 65-71.
37. K. Sato *et al*. in preparation
38. I.D. Brown and D. Altermatt, *Acta Cryst.*, 1985, **B41**, 244-247.
39. P. Kubelka and F. Munk, *Zeit*. *Für*. *Tekn*. *Physik*., 1931, **12**, 593-601.
40. Z.V. Marinković Stanojević, N. Romčević and B. Stojanović, *J. Eur. Ceram. Soc*. 2007, **27**, 903-907.
41. D. de Waal, *Asian. Chem. Lett.*, 2004, **8**, 57-63.
42. C.M. Julien, F. Gendron, A. Amdouni and M. Massot, *Mater*. *Sci*. *Eng*. *B-Solid*., 2006, **130**, 41-48.
43. N. W. Grimes and A. J. Collett, *Phys*. *Stat*. *Sol*. *B*, 1971, **43**, 591−599.
44. H. Shirai, Y. Morioka and I. Nakagawa, *J. Phys*. *Soc*. *Jpn*., 1982, 52, 592-597.
45. P. C. Garcia and I. Rasines, *J. Solid State Chem*., 1984, **52**, 187−193.
46. H. D. Lutz, B. Müller and H. J. Steiner, *J. Solid State Chem*., 1991, **90**, 54−60.
47. Z. P. Xu and H. C. Zeng, *J. Mater*. *Chem*., 1998, **8**, 2499−2506.
48. I. Broussell, E. Fortin, L. Kulyuk, S. Popov, A. Anedda and R. Corpino, *J. Appl*. *Phys*., 1998, **84**, 533-540
49. M.G. Brik, N.M. Avram, C.N. Avram, C. Rudowicz, Y.Y. Yeung and P. Gunutek, *J. Alloy*. *Compound*, 2007, **432**, 61-68.
50. L.K.C.de Souza, J.R. Zamian, G.N. da Rocha Filho, L.E.B. Soledade, I.M.G. dos Santos, A.G. Souza, T. Scheller, R.S. Angélica and C.E.F. da Costa, *Dyes and Pigments*, 2009, **81**, 187-192.
51. H. Dixit, N. Tandon, S. Cottenier, R. Saniz, D. Lamoen and B. Partoens, *Phys*. *Rev*. *B*, 2013, **87**, 174101/1-7.

